Journal of Advanced Research 22 (2020) 77–84

Contents lists available at ScienceDirect

Journal of Advanced Research

journal homepage: www.elsevier.com/locate/jare

$CuBr_2$/EDTA-mediated ATRP for ultrasensitive fluorescence detection of lung cancer DNA

Jingyu Zhang [a], Yanyan Ba [a], Qianrui Liu [c], Liying Zhao [a], Dazhong Wang [b,*], Huaixia Yang [a,*], Jinming Kong [c,*]

[a] Pharmacy College, Henan University of Chinese Medicine, Zhengzhou 450008, PR China
[b] People's Hospital of Zhengzhou, Zhengzhou 450008, PR China
[c] School of Environmental and Biological Engineering, Nanjing University of Science and Technology, Nanjing 210094, PR China

GRAPHICAL ABSTRACT

An ultrasensitive fluorescence method for early diagnosis of lung cancer via activators regenerated by electron transfer atom transfer radical polymerization (ARGET-ATRP) with EDTA as metal ligand was reported.

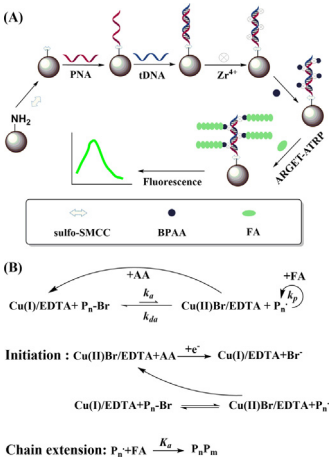

ARTICLE INFO

Article history:
Received 29 August 2019
Revised 8 November 2019
Accepted 13 November 2019
Available online 16 November 2019

Keywords:
EDTA
Fluorescence detection
CYFRA21-1

ABSTRACT

In this paper, we reported a system for the ultrasensitive fluorescence detection of cytokeratin fragment antigen 21–1 DNA (CYFRA21-1 DNA) for the early diagnosis of lung cancer. The approach used electron transfer atom transfer radical polymerization (ARGET-ATRP) with ethylenediaminetetraacetic acid (EDTA) as the metal ligand. Firstly, thiolated peptide nucleic acid (PNA) was linked to aminated magnetic beads solutions (MBs) by a cross-linking agent and then hybridized with CYFRA21-1 DNA (tDNA). Subsequently, Zr^{4+} was introduced into the MBs by conjugating with the phosphate group of tDNA, and the initiator of ARGET-ATRP was introduced into via phosphate-Zr^{4+}-carboxylate chemistry. Next, Cu(II)Br/EDTA was reduced to Cu(I)/EDTA by ascorbic acid (AA) to trigger ARGET-ATRP and then a large amount of fluorescein-o-acrylate (FA) molecules were grafted from the surface of the MBs, which

Peer review under responsibility of Cairo University.
* Corresponding authors.
E-mail addresses: wdzlion_fox@163.com (D. Wang), yhx998@hactcm.edu.cn (H. Yang), j.kong@njust.edu.cn (J. Kong).

https://doi.org/10.1016/j.jare.2019.11.006
2090-1232/

ARGET-ATRP
Lung cancer

amplified significantly the fluorescent signal. Under optimal conditions, a strong linear relationship of tDNA over the range from 0.1 fM to 1 nM (R^2 = 0.9988). The limit of detection was as low as 23.8 aM (~143 molecules). The fluorescence detection based on the ARGET-ATRP strategy yielded excellent sensitivity, selectivity, outstanding anti-interference properties, and cost-effectiveness. These results indicated that this strategy has considerable potential for biological detection and early clinical diagnosis.

Introduction

Due to the low abundance of biomolecules in human serum and the difficulty of directly detecting these biomolecules, efforts have been made over many years to find suitable strategies for signal amplification. In recent years, atom transfer radical polymerization (ATRP) has been applied to signal amplification [1–4], due to its well-controlled reaction rate, the availability of a wide range of monomers and its simplicity of operation. Recently, research into ATRP has focused on its environmental impacts. The ligands and transition metals used are harmful to both human beings and the environment. There are various metal ligands of ATRP, including poly (ethylene imine), and N,N,N′,N″,N″-pentamethyldiethylene triamine (PMDETA) [5–7], tris (2-(dimethylamino)ethyl) amine (Me_6TREN) [8–10] and so on. Ethylenediaminetetraacetic acid (EDTA) is a chelating agent [11], is cost-effective, and has stable performance and low toxicity. EDTA can form stable water-soluble complexes with alkali metals, rare earth elements, and transition metals [12]. EDTA, as a multidentate ligand containing more than two coordination atoms can form a metal complex with metal ions. The complexes formed by EDTA and most metal ions have the characteristics of high stability, a simple coordination ratio (generally 1:1), rapid coordination reaction, and good water solubility. Therefore, EDTA has considerable practical value. In recent years, the application of complexes in molecular detection has attracted great attention. The $FeCl_2$/EDTA-system has been studied as an ATRP mediator [13,14].

The regulation of ATRP involves activators regenerated by electron transfer atom transfer radical polymerization (ARGET-ATRP) [15–17], photo ATRP [18,19] and mechano ATRP [20,21]. As a number of the ATRP family, ARGET-ATRP requires low concentrations of transition catalysts, and can react under low oxygen conditions, due to the excess of reducing agent [22–24]. ARGET-ATRP has been gradually used in the fields of industry, biology, pharmacy, and environmental science [22,25]. ARGET-ATRP can establish a reversible dynamic equilibrium between Cu (II), the dormant species, and Cu (I) the active species, by a reducing agent, with a large amount of monomer repeatedly added to achieve polymerization [26,27]. Previous researchers have reported the use of ARGET-ATRP as an amplification technique for achieving ultrasensitive detection of biomolecules. Cheng et al. had reported synthesis of a surface-active ATRP initiator, and its use in ARGET-ATRP polymerisation [17].

In this paper, we report the development of an ultrasensitive fluorescent CYFRA21-1 DNA detection for the early diagnosis of lung cancer based on ARGET-ATRP with EDTA as the metal ligand. CYFRA21-1 DNA is considered as the most important biomarker of the diagnosis of non-small cells (NSCLC), which is commonly used as the tDNA to diagnosis NSCLC. Thiolated peptide nucleic acid (PNA) was modified on the surface of the MBs by a cross-linking agent. Next, CYFRA21-1 segments were specifically identified using PNA. After hybridization between PNA and tDNA, α-bromophenylacetic acid (BPAA), the initiator of ARGET-ATRP, was linked to the PNA/DNA heteroduplexes via bridges of phosphate-Zr^{4+}-carboxylate chemistry. Subsequently, EDTA was used as the metal ligand of Cu(II), and Cu(II)Br/EDTA was formed. Ascorbic acid (AA), as the catalyst of ARGET-ATRP reduced Cu(II)Br/EDTA to Cu (I)/EDTA for activating polymerization, and numerous monomers (fluorescein-o-acrylate) were introduced to the surface of the MBs. This strategy produced a strong linear relationship between the fluorescence signal and the logarithm of tDNA concentrations between 0.1 fM and 1 nM, with a low detection limit. This strategy has excellent stability, cost-effectiveness, selectivity, and outstanding anti-interference properties. This signal amplification strategy based on ARGET-ATRP with EDTA as the metal ligand was firstly reported in the field of sensing analysis.

Experimental section

Materials and reagents

All chemicals and reagents were analytical grade, and ultrapure water was used in all experiments. Aminated magnetic beads solutions (MBs, 10 mg mL^{-1}) were procured from PuriMag Biotech Co., Ltd. (Xiamen, China). Ethylenediaminetetraacetic acid disodium salt (EDTA) was obtained from Beijing Solarbio Science&Technology Co., Ltd. (Beijing, China). Ascorbic acid (AA), 4-(N-maleimidomethyl)cyclohexane-1-carboxylic acid 3-sulfo-N-hydroxysuccinimide ester sodium salt (sulfo-SMCC), and zirconium dichloride oxide octahydrate ($ZrOCl_2$) were obtained from J&K Scientific Ltd. (Beijing, China). Fluorescein-o-acrylate (FA) and α-bromophenylacetic acid (BPAA) were purchased from Sigma-Aldrich (St. Louis, USA). *N,N*-dimethylformamide (DMF) and copper (II) bromide ($CuBr_2$) were purchased from Sinopharm Chemical Reagent Co., Ltd. (Shanghai, China). Sodium hydroxide, sodium dihydrogen phosphate, sodium chloride and disodium hydrogen phosphate were obtained from Tianjin Kemeo Chemical Test Co., Ltd. (Tianjin, China). Normal human serum (NHS) was produced by Shanghai YiJi Industrial Co., Ltd. (Shanghai, China). All oligonucleotides were purchased from Sangon Biotechnology Co., Ltd. (Shanghai, China). As shown in Table 1, the sequences of oligonucleotides were displayed.

Table 1
Sequences of PNA and SSDNA used.

Synthetic oligonucleotide	Base sequences (5′-3′)
Peptide nucleic acid (PNA)	SH-$(CH_2)_{11}$-(O linker)$_3$-GAAGGGAGGAATGGTGTCAGGGGCG
Target complementary DNA (tDNA)	CGCCCCTGACACCATTCCTCCCTTC
Single base mismatched DNA (SBM)	CGCCCCTAACACCATTCCTCCCTTC
Three bases mismatched DNA (TBM)	CGCCCATGACACTATTCCTCGCTTC
Control DNA (Control)	TATTATCCGTCAGTGGAAAGGACCG

Phosphate buffer saline (PBS butter, 0.1 M, pH 7.4) was used for diluting and washing oligonucleotides, and the solvent for the fluorescence detection was prepared using 0.1 M PBS butter.

Apparatus

All modifications of MBs were carried out on a constant temperature shaker (St. Louis, USA). The atomic force microscope (AFM) images were obtained from Dimension Icon (Bruker, USA). Fluorescent measurements were recorded using an Edinburgh FLS-1000 fluorescence spectrophotometer (Edinburgh, UK). Scanning electron microscopy (SEM) images were obtained with Sigma HD field emission SEM (Zeiss, Germany).

PNA functionalization of MBs

Prior to use, 20 μL of MBs were washed three times, and then PBS buffer (pH 7.4, 0.1 M, 180 μL) was added to resuspend the MBs in a centrifuge tube. Subsequently, sulfo-SMCC (0.5 mM, 20 μL) were added to the centrifuge tubes respectively and mixed completely, and the reaction was carried out at 310 K for 2 h in a constant temperature shaker.

After washing with PBS buffer (pH 7.4, 0.1 M) the mixture was magnetically separated. The MBs were distributed in PNA (0.5 μM, 5 μL) and PBS buffer (pH 7.4, 0.1 M, 195 μL), and the reaction solution was placed in the constant temperature shaker at 310 K overnight.

Modification of sulfo-SMCC/PNA/DNA/Zr^{4+}-modified MBs

After washing and magnetically separation in PBS buffer (pH 7.4, 0.1 M), tDNA (0.1 nM, 20 μL) and PBS buffer (pH 7.4, 0.1 M, 180 μL) were added to the centrifuge tube respectively and mixed completely. Afterwards, the reaction was incubated for two hours at 310 K in the constant temperature shaker. Subsequently, the MBs were washed with PBS butter (pH 7.4, 0.1 M), the MBs were reacted with Zr^{4+} (0.5 mM, 20 μL) and PBS buffer (pH 7.4, 0.1 M, 180 μL). After then, the reacting system was placed in the constant temperature shaker for 0.5 h at 310 K. Finally, the sulfo-SMCC/PNA/DNA/Zr^{4+}-modified MBs were formed.

$CuBr_2$/EDTA-mediated ARGET-ATRP

To produce the initiator-modified MBs, the sulfo-SMCC/PNA/DNA/Zr^{4+}-modified MBs were washed and magnetically separated in PBS buffer (pH 7.4, 0.1 M). Next, BPAA (1 mM, 20 μL) and PBS buffer (pH 7.4, 0.1 M, 180 μL) were added to the reaction system at 310 K for 1 h. The sulfo-SMCC/PNA/DNA/Zr^{4+}/BPAA-modified MBs were obtained. This ARGET-ATRP mixture was obtained by adding FA (10 mM, 10 μL), AA (2 mM, 20 μL), and Cu(II)Br/EDTA (10 mM, 20 μL, 1:1.2 in molarity dissolved in DMF) into PBS buffer (pH 7.4, 0.1 M, 150 μL). Then the ARGET-ATRP mixture was added to the reacting system and placed in a constant temperature shaker at 310 K for 2 h to obtain the sulfo-SMCC/PNA/DNA/Zr^{4+}/BPAA/FA-modified MBs.

Fluorescent detection of CYFRA21-1 DNA

The sulfo-SMCC/PNA/DNA/Zr^{4+}/BPAA/FA-modified MBs from ARGET-ATRP were washed with DMF, and PBS buffer (pH 7.4, 0.1 M) in succession, and magnetically separated. Finally, the fluorescence intensity was measured by adding sulfo-SMCC/PNA/DNA/Zr^{4+}/BPAA/FA-modified MBs sample into 700 μL of PBS buffer (pH 7.4, 0.1 M). The fluorescent signals were amplified using a fluorospectrophotometer with an excitation wavelength of 489 nm, and a slit width of 2 nm.

Results and discussion

Principle of the fluorescence sensor via $CuBr_2$/EDTA-mediated ATRP

The process of construction of this ultrasensitive fluorescence sensor based on ARGET-ATRP with EDTA as the metal ligand was showed in Fig. 1. During this process, first of all, PNA capture probes were immobilized on the surface of MBs with sulfo-SMCC. The carbonyl group of the sulfo-SMCC was connected with the MBs-NH_2 to link the sulfo-SMCC to the surface of the MBs. The double bond at the other end of the sulfo-SMCC reacted with the sulfydryl group of PNA by an addition reaction, and a PNA probe was modified to the surface of MBs. PNA can hybridize with tDNA to form PNA/DNA heteroduplexes through specifically identifying between PNA and tDNA. Subsequently, under the coordination of Zr^{4+}, the phosphate groups of tDNA and the carboxy group of the initiator (BPAA) were coordinated with Zr^{4+} to form sulfo-SMCC/PNA/tDNA/Zr^{4+}/BPAA-modified MBs.

At the beginning of ARGET-ATRP, Cu(II)Br/EDTA was reduced to Cu(I)/EDTA by AA, and AA was oxidated to dehydroascorbic acid (DHA). The Br^- of BPAA was seized by Cu(I)/EDTA while Cu(II)Br/EDTA was produced due to the transfer of Br from BPAA to Cu(I)/EDTA, and free radical (P•) was generated. The regenerated Cu(II)Br/EDTA was again reduced to Cu(I)/EDTA by excessive AA, and P• continuously attacked the carbon-carbon double bond of the monomer (FA), and polymer chains were formed.

In this study, EDTA was used as the ligand of Cu(II) to form strong complexes with Cu(I) and Cu(II). EDTA is widely used as multidentate ligand [28,29], due to it being a reagent with N and O

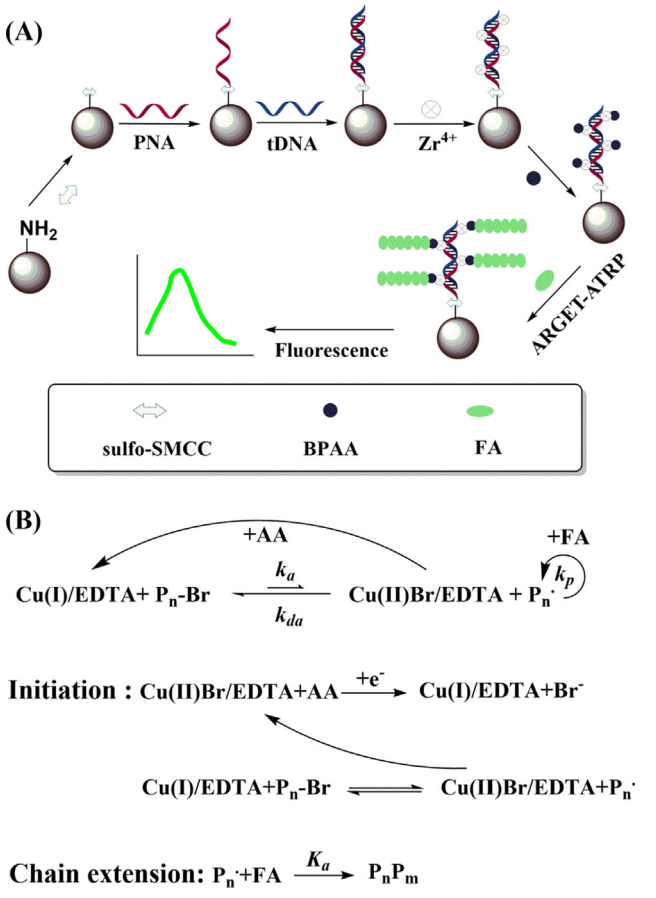

Fig. 1. Schematic illustration of fluorescent biological analysis based on ARGET-ATRP with EDTA as the metal ligand (A). Principle of the ARGET-ATRP with EDTA as the metal ligand strategy (B).

complexing points. It exists as a double dipole ion structure in aqueous solution, so when the concentration of OH^- increased, the H^+ decreased and the concentration of (ethylenediamine tetraacetic acid root) Y^{4-} increased in EDTA aqueous solution. Because of each N atom of EDTA had two lone pair electrons, each of the O atoms had two lone pair electrons when Y^{4-} was at higher concentration in EDTA aqueous solution. The concentration of OH^- is greater than H^+ in aqueous solution, Y^{4-} was the most abundant ion species in the aqueous solutions. Thus, Y^{4-} had six coordination atoms when the aqueous solution was alkaline. In the ARGET-ATRP system, Cu(II)Br with EDTA formed (Cu(II)Br/EDTA) complexes, which formed Cu(I)/EDTA, under the action of the reducing agent AA. Because PBS buffer (pH 7.4, 0.1 M) was used in all experiments, the stability of the Cu(II)Br/EDTA and Cu(I)/EDTA complexes was not affected, and the growth of the polymeric chains was stable.

Feasibility of the fluorescence biosensor

In order to explore the feasibility of this ultrasensitive DNA fluorescent detection via ARGET-ATRP with EDTA as the metal ligand, we compared the fluorescence intensity of the MBs that were modified with different materials. As shown in the Fig. 2, the fluorescence signal near zero when the PBS buffer (curve a) was detected, the result shown that the fluorescence signal of modified MBs was not affected by adding PBS buffer. The proposed sulfo-SMCC/PNA/tDNA/Zr^{4+}/BPAA/FA-modified MBs (curve g) generated the strongest fluorescence intensity at 512 nm. Under other conditions (in the absence of PNA, tDNA, Zr^{4+}, BPAA, or FA, respectively), the fluorescence signal was particularly weak. In the absence of FA (curve b), the fluorescence intensity was almost zero. This could be because FA could not be introduced to MBs utilizing ARGET-ATRP, so the fluorescent signal was not successfully amplified. The fluorescence intensity was also very low when the BPAA initiator (curve f) was not added, due to the lack of free radicals. In addition, very weak fluorescence intensities were observed without PNA (curve c), tDNA (curve d) or Zr^{4+} (curve e), because the polymer resulting from the ARGET-ATRP reaction could not be connected to the surface of the MBs. These experiments clearly demonstrated the importance of PNA and DNA complementary pairing, and also illustrated that the strategy had a high signal-to-noise (S/N) ratio and showed high sensitivity for tDNA. Therefore, the experimental results indicated that the amplified signal produced by a strategy based on ARGET-ATRP with EDTA as the metal ligand could be applied to the detection of CYFRA21-1 of lung cancer.

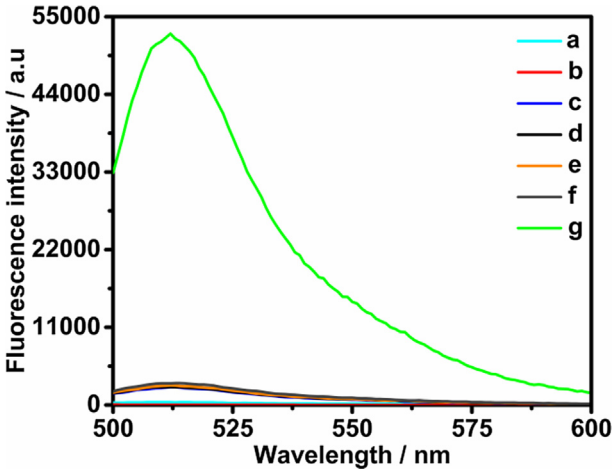

Fig. 2. Feasibility of ultrasensitive fluorescent tDNA detection. Fluorescence spectra of sulfo-SMCC/PNA/tDNA/Zr^{4+}/BPAA/FA-modified MBs (curve g), PBS buffer (a), and in the absence of PNA (c), tDNA (d), Zr^{4+} (e), BPAA (f), and FA (b)-modified MBs. (Ex = 489 nm, slit: 2 nm).

Characterization of MBs modification

AFM was used to verify the surface morphology of the modified MBs. Fig. 3 showed that the height of the sulfo-SMCC/PNA/tDNA/Zr^{4+}/BPAA/FA-modified MBs was 32.4 nm, while the sulfo-SMCC/PNA-modified MBs showed a maximum height of 9.3 nm. By contrast the height of different modified MBs, we found the sulfo-SMCC/PNA/tDNA/Zr^{4+}/BPAA/FA and sulfo-SMCC/PNA-modified MBs had a dramatic change of height. The reason for this result might be that the monomer (FA) was aggregated on the surface of MBs via ARGET-ATRP. However, if tDNA was absent from the system, the phosphate-Zr^{4+}-carboxylate chemistry was disabled leading to unsuccessful polymerization. As displayed in Fig. 4(A, B), SEM investigation revealed that the sulfo-SMCC/PNA/tDNA/Zr^{4+}/BPAA/FA-modified MBs (Fig. 4A) had a relatively rough surface compared with that of the control group without tDNA (Fig. 4B), and floccule was observed on the surface of the functional MBs. Those results suggested that this signal amplification strategy using the $CuBr_2$/EDTA-system as an ATRP mediator was feasible.

To further characterize the biosensor, energy dispersive spectroscopy (EDS) was applied to observe the elements on the surface of the MBs for qualitative analysis. Different elements possesses different frequency of characteristic X-rays [30,31]. Therefore, the different elements appear in different colors when EDS was used to scan the surface of a sample with an electron beam. As shown in Fig. 4(C-F), the EDS images of the MBs showed that the characteristic element composition was S (Fig. 4C) P, (Fig. 4D), Zr (Fig. 4E), and Br (Fig. 4F). The S element exists in PNA, hence, the results showed that PNA was present on the surface of the MBs. The P element in EDS images was shown because of the phosphate groups of tDNA, indicating that tDNA was successfully attached to the surface of the MBs by the PNA capture probe. The presence of Zr and Br element indicated that $ZrOCl_2$ and BPAA were successfully attached to the surface of the MBs via phosphate-Zr^{4+}-carboxylate chemistry. From these results, we could see that the ultrasensitive fluorescence sensor using the $CuBr_2$/EDTA-system as an ATRP mediator was successfully constructed.

Optimization of ARGET-ATRP conditions

In order to achieve ultrasensitive analysis of CYFRA21-1 via fluorescence sensors, various conditions of detection of ARGET-ATRP most be taken into account, including the reaction time of AGTE-ATRP and the amount of FA. The growth of ARGET-ATRP polymeric chains was correlated with the coupling time of probes onto the MBs surface. Therefore, the relationship between the fluorescence intensity and the reaction time of AGTE-ATRP was investigated. As shown in Fig. S1A, with increasing time, the fluorescence intensity rapidly increased from 10 min to 100 min, after which the fluorescence intensity reached a plateau. Presumably, the growth of the polymer chain was terminated, which might be because the reaction had reached equilibrium. Hence, the ideal reaction time of ARGET-ATRP for the subsequent experiments was set to 100 min.

In this method, the amount of fluorescence monomer (FA) introduced into the MBs affected the length of the ARGET-ATRP chain. In Fig. S1B, it clearly showed that the fluorescence signal intensity did not increase until the volume of FA was more than 10 μL, which could indicate that the reaction of ARGET-ATRP had stopped. To further improve the cost-effectiveness of the fluorescence sensors, the optimal amount of FA was determined to be 10 μL, an amount that was used in the subsequent experiments.

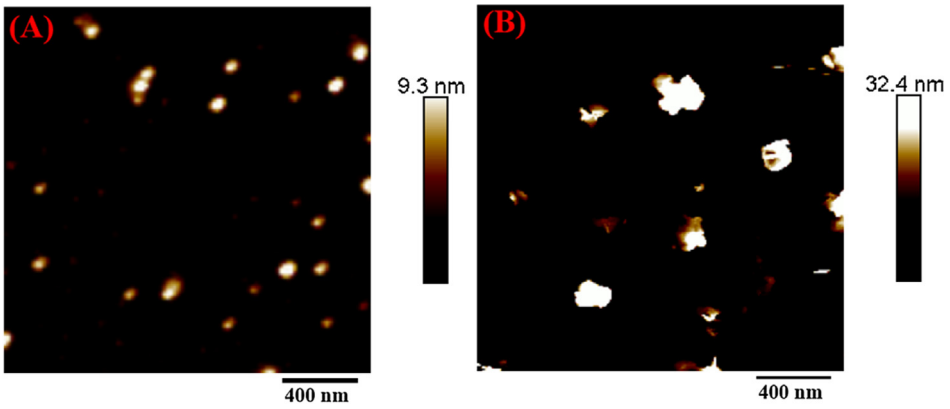

Fig. 3. AFM images of differently-modified MBs. The image of sulfo-SMCC/PNA-modified MBs (A) and sulfo-SMCC/PNA/tDNA/Zr^{4+}/BPAA/FA-modified MBs (B).

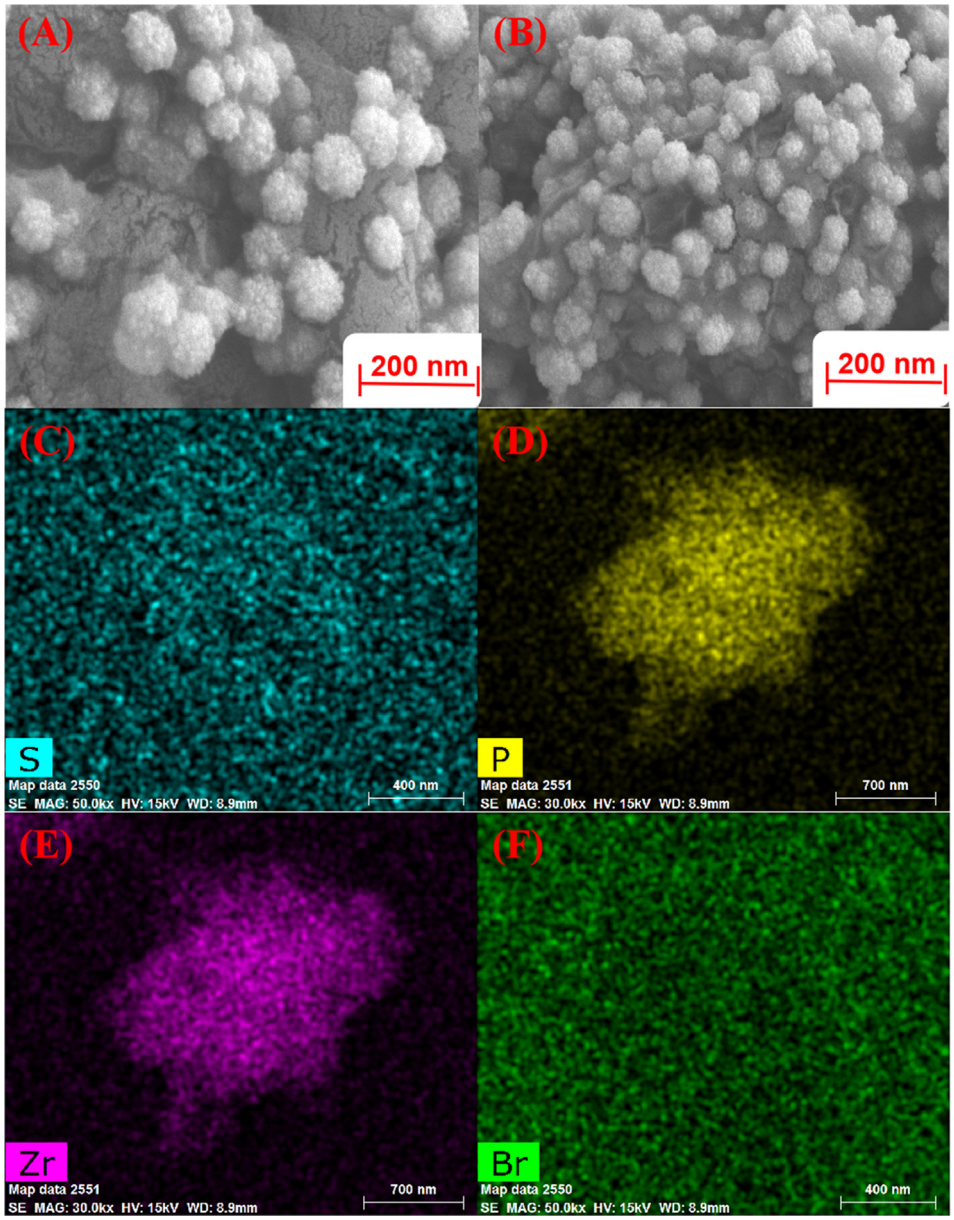

Fig. 4. SEM and EDS images of differently-modified MBs. SEM images of sulfo-SMCC/PNA-modified MBs (A) and sulfo-SMCC/PNA/tDNA/Zr^{4+}/BPAA/FA-modified MBs (B). EDS figures of sulfo-SMCC/PNA/tDNA/Zr^{4+}/BPAA/FA-modified MBs. Images of the elements S (C), P (D), Zr (E), Br (F).

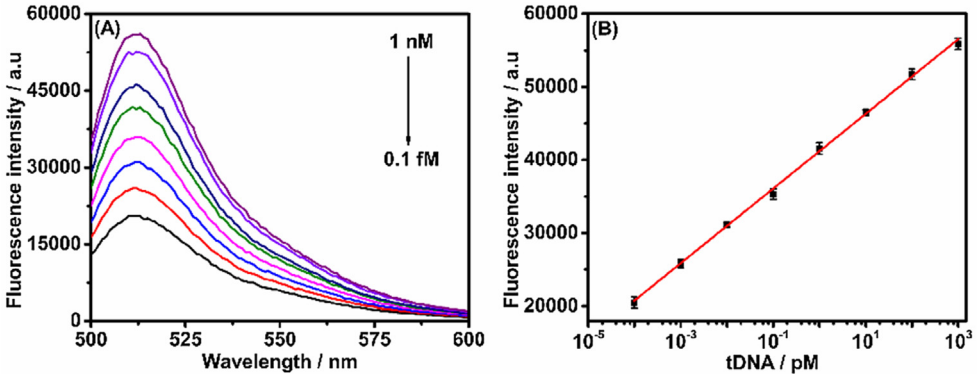

Fig. 5. Fluorescence spectra of different tDNA concentrations (0.1 fM, 1 fM, 10 fM, 0.1 pM, 1 pM, 10 pM, 0.1 nM, and 1 nM) (A). Calibration plot between the logarithm of tDNA concentration from 0.1 fM to 1 nM and the fluorescence intensity (B). (Ex = 489 nm, Em = 512 nm, pH = 7.4, 0.1 M PBS butter), The error bars represent the standard deviation of four measurements.

Table 2
Comparison of our method and other developed detection methods.

Detection method	L.R. (M)	D.L. (M)	Reference
Electrochemistry	$1.0 \times 10^{-12} \sim 5.0 \times 10^{-6}$	1.5×10^{-13}	[32]
Electrochemistry	$1.0 \times 10^{-9} \sim 1.0 \times 10^{-7}$	1.0×10^{-10}	[33]
Electrochemistry	$1 \times 10^{-10} \sim 1.0 \times 10^{-6}$	1.0×10^{-11}	[34]
Fluorescence	$1 \times 10^{-15} \sim 1 \times 10^{-8}$	5×10^{-16}	[35]
Fluorescence	$2.3 \times 10^{-10} \sim 2.3 \times 10^{-8}$	1.15×10^{-10}	[36]
Fluorescence	$6.0 \times 10^{-13} \sim 2.4 \times 10^{-10}$	6×10^{-14}	[37]
Fluorescence	$3.0 \times 10^{-9} \sim 1.2 \times 10^{-7}$	2.0×10^{-9}	[38]
Fluorescence	$1.0 \times 10^{-16} \sim 1.0 \times 10^{-9}$	2.38×10^{-17}	This work

Analytical performance for CYFRA21-1 DNA detection

Under the optimum experimental conditions, in order to explore the analytical performance of the fluorescence CYFRA21-1 DNA biosensor based on the ARGET-ATRP signal amplification strategy, we investigated the relationship between fluorescence intensity and various concentrations of tDNA. As shown in Fig. 5A, the fluorescence absorption was strongest at 512 nm. The fluorescence intensity gradually increased with the increase of the concentration of tDNA in the range of 0.1 fM to 1 nM. As shown in Fig. 5B, the liner regression equation was F (au) = 5108.56 lgC_{tDNA} + 41197.29, with a correlation coefficient (R^2) of 0.9988, and the detection limit (LOD) of this method was calculated to be 23.8 aM based on the S/N = 3. To further demonstrate the excellent performance of the fluorescence biosensor, as summarized in Table 2, we compared the linear range and LOD of this strategy to that of other sensors. This method improved the detection sensitivity of the fluorescence DNA biosensor by taking advantage of specific recognition of PNA probes and ATRP amplification. This strategy also had the advantages of low cost and simple operation.

Selectivity, stability, and anti-interference ability

Selectivity and stability are important parameters for evaluating the performance of this biosensor. In order to demonstrate the selectivity of the fluorescence DNA biosensor, we tested and compared the fluorescence intensity of 0.1 nM tDNA with that of 0.1 nM SBM, TBM, and Control under the same conditions. In Fig. 6A, it could be seen that the fluorescence intensity of the Control, TBM, and SBM were respectively 93.69%, 83.46%, and 80.82% lower than that of tDNA. The mismatched base(s) of those oligonucleotides were unfavorable for the forming of PNA/DNA heteroduplexes, which led to the reduction of phosphate and thus the reduction of ATRP initiator. The amount of monomers dramatically decreased, therefore the fluorescence intensity of the Control, TBM, and SBM decreased. These results demonstrated that the DNA fluorescence detection system was able to specifically detect DNA, and the fluorescence biosensor had high selectivity for DNA.

The stability of this fluorescence biosensor was demonstrated by testing the fluorescence intensity of sulfo-SMCC/PNA/tDNA/Zr^{4+}/BPAA/FA-modified MBs. Under the same experimental conditions, the MBs samples were stored for two weeks at 4 °C, then the samples were uniformly mixed. The fluorescence intensity of the MBs showed no significant change. Therefore, the results indi-

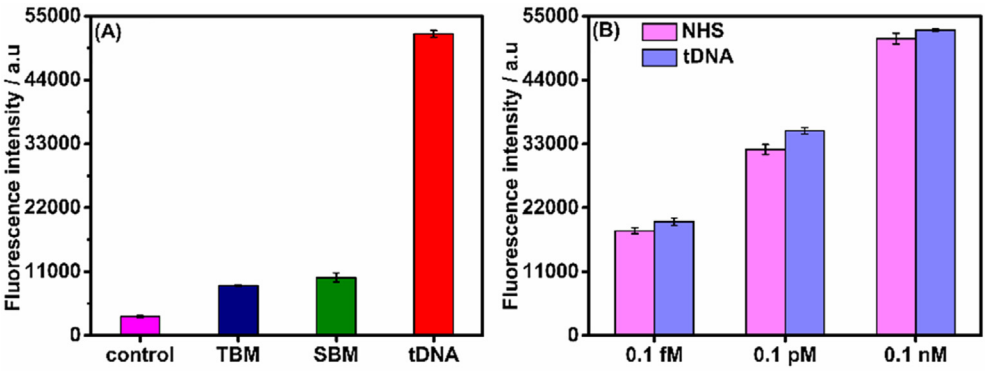

Fig. 6. Fluorescence intensity of this fluorescence biosensor toward tDNA, SBM, TBM, and Control (with a concentration of 0.1 nM) (A). Fluorescence response of tDNA with concentrations of 0.1 nM, 0.1 pM and 0.1 fM in PBS buffer or 5% NHS (B). The error bars represent the standard deviation of four measurements.

cated that the DNA fluorescence biosensor had satisfactory stability.

In order to evaluate the anti-interference ability of this fluorescence DNA biosensor in normal human serum, the fluorescence intensity in 0.1 fM, 0.1 pM, and 0.1 nM tDNA in 5% NHS were compared with those in PBS buffer. As shown in Fig. 6B, the fluorescence intensity of 0.1 fM, 0.1 pM and 0.1 nM tDNA in 5% NHS were approximately 91.99%, 90.87%, and 97.15% of those from PBS butter (pH 7.4, 0.1 M), respectively. Hence, the fluorescence biosensor based on the ARGET-ATRP signal amplification strategy had an excellent anti-interference ability in NHS and had a good potential for application potential in a clinical setting.

Conclusions

We have reported an ultrasensitive fluorescence biosensor based on ARGET-ATRP signal amplification with EDTA as the metal ligand, and applied it to the detection of CYFRA21-1 of lung cancer for the first time. Under optimum reaction conditions, this fluorescence biosensor shows a good analytical performance, with a linear range of 0.1 fM to 1 nM, and a detection limit is as low as 23.8 aM. The most important reason for this performance is that the method exhibited displays high anti-interference ability in capability NHS. However, it has some deficiencies that need to be further improved. For example, optimization of the total assay time for biosensor applications would be valuable. In summary, because of the fluorescence sensor's low cost, good selectivity, excellent anti-interference capability, high stability, and good sensitivity, the fluorescence sensor showed great promise for the detection of clinically important entities, such as those involved in cancer.

Compliance with ethics requirements

This article does not contain any studies with human or animal subjects.

Declaration of Competing Interest

The authors declare that they have no known competing financial interests or personal relationships that could have appeared to influence the work reported in this paper.

Acknowledgements

This work was supported by the project of tackling of key scientific and technical problems in Henan Province (192102310033); the National Natural Science Foundation of China (21575066); the Henan University of traditional Chinese medicine, China of graduate student innovation project (YJS2018B10).

Appendix A. Supplementary material

Supplementary data to this article can be found online at https://doi.org/10.1016/j.jare.2019.11.006.

References

[1] Hu Q, Wang Q, Sun G, Kong J, Zhang X. Electrochemically mediated surface-initiated de novo growth of polymers for amplified electrochemical detection of DNA. Anal Chem 2017;89(17):9253–9.
[2] Sikes HD, Hansen RR, Johnson LM, Jenison R, Birks JW, Rowlen KL, et al. Using polymeric materials to generate an amplified response to molecular recognition events. Nat Mater 2008;7(1):52.
[3] Chen F, Hou S, Li Q, Fan H, Fan R, Xu Z, et al. Development of atom transfer radical polymer-modified gold nanoparticle-based enzyme-linked immunosorbent assay (ELISA). Anal Chem 2014;86(20):10021–4.
[4] He P, Lou X, Woody SM, He L. Amplification-by-polymerization in biosensing for human genomic DNA detection. ACS Sensors 2019;4(4):992–1000.
[5] Zhou Y, Wang K, Hu D. High retreatability and dimensional stability of polymer grafted waterlogged archaeological wood achieved by ARGET ATRP. Sci Rep 2019;9(1):9879.
[6] Kermani SF, Taromi FA. The effects of catalyst and deactivator species in atom transfer radical polymerization of n-butyl methacrylate. Iran Polym J 2019;28(5):361–70.
[7] Gan W, Cao X, Shi Y, Zou L, Gao H. Ligand effect in the synthesis of hyperbranched polymers via copper-catalyzed azide-alkyne cycloaddition polymerization (CuAACP). J Polym Sci, Part A: Polym Chem 2018;56(19):2238–44.
[8] Guo JK, Zhou YN, Luo ZH. Electrochemically mediated ATRP process intensified by ionic liquid: A "flash" polymerization of methyl acrylate. Chem Eng J 2019;372:163–70.
[9] Su X, Jessop PG, Cunningham MF. ATRP catalyst removal and ligand recycling using CO_2-switchable materials. Macromol 2018;51(20):8156–64.
[10] Wang L, Li Z, Huang P, Ding W. Synthesis of an acrylamide copolymer containing nano-SiO_2 by ex situ Cu(0)-mediated SET-LRP. Int J Polym Sci 2019;2019:1–7.
[11] Wang Z, Wu S, He Z. Production of electricity and water in an osmotic microbial fuel cell by using EDTA-Na_2 as a recoverable draw solute. Sci Total Environ 2019;677:382–9.
[12] Mudsainiyan RK, Jassal AK, Chawla SK. New water soluble heterometallic complex showing unpredicted coordination modes of EDTA. J Solid State Chem 2015;230:61–9.
[13] Bergenudd H, Jonsson M, Nyström D, Malmström E. Heterogeneous iron (II)-chloride mediated radical polymerization of styrene. J Mol Catal A: Chem 2009;306(1–2):69–76.
[14] Wang G, Lu M, Wu H. SET LRP of MMA mediated by Fe(0)/EDTA in the presence of air. Polym Bull 2012;69(4):417–27.
[15] He P, Zheng W, Tucker EZ, Gorman CB, He L. Reversible addition−fragmentation chain transfer polymerization in DNA biosensing. Anal Chem 2008;80(10):3633–9.
[16] Wu Y, Liu S, He L. Electrochemical biosensing using amplification-by-polymerization. Anal Chem 2009;81(16):7015–21.
[17] Cheng CJ, Fu QL, Bai XX, Liu SJ, Shen L, Fan WQ, et al. Facile synthesis of gemini surface-active ATRP initiator and its use in soap-free AGET ATRP mini-emulsion polymerisation. Chem Pap 2013;67(3):336–41.
[18] Konkolewicz D, Schröder K, Buback J, Bernhard S, Matyjaszewski K. Visible light and sunlight photoinduced ATRP with ppm of Cu catalyst. ACS Macro Lett 2012;1(10):1219–23.
[19] Whitfield R, Parkatzidis K, Rolland M, Truong N, Anastasaki A. Tuning dispersity by photo-induced ATRP: Monomodal distributions with ppm copper concentration. Angewandte Chemie International Edition. Angew Chem Int Ed 2019. doi: https://doi.org/10.1002/anie.201906471.
[20] Mohapatra H, Kleiman M, Esser-Kahn AP. Mechanically controlled radical polymerization initiated by ultrasound. Nat Chem 2017;9(2):135.
[21] Jia Y, Wang WJ, Li BG, Zhu S. Design and synthesis of mechano-responsive color-changing thermoplastic elastomer based on poly (n-butyl acrylate)-spiropyran-polystyrene comb-structured graft copolymers. Macromol Mater Eng 2018;303(9):1800154.
[22] Li X, Wang WJ, Li BG, Zhu S. Kinetics and modeling of solution ARGET ATRP of styrene, butyl acrylate, and methyl methacrylate. Macromol React Eng 2011;5(9–10):467–78.
[23] Patra S, Roy E, Das R, Karfa P, Kumar S, Madhuri R, et al. RETRACTED: Bimetallic magnetic nanoparticle as a new platform for fabrication of pyridoxine and pyridoxal-5′-phosphate imprinted polymer modified high throughput electrochemical sensor. Biosens Bioelectron 2015;122:301.
[24] Vidiella del Blanco M, Gomez V, Keplinger T, Cabane E, Morales LFG. Solvent-controlled spatial distribution of SI-AGET-ATRP grafted polymers in lignocellulosic materials. Biomacromolecules 2018;20(1):336–46.
[25] Zhang Z, Wang X, Tam KC, Sèbe G. A comparative study on grafting polymers from cellulose nanocrystals via surface-initiated atom transfer radical polymerization (ATRP) and activator re-generated by electron transfer ATRP. Carbohydr Polym 2019;205:322–9.
[26] Forbes DC, Creixell M, Frizzell H, Peppas NA. Polycationic nanoparticles synthesized using ARGET ATRP for drug delivery. Eur J Pharm Biopharm 2013;84(3):472–8.
[27] Ma W, Otsuka H, Takahara A. Poly (methyl methacrylate) grafted imogolite nanotubes prepared through surface-initiated ARGET ATRP. Chem Commun 2011;47(20):5813–5.
[28] Boland NE, Stone AT. Rates of nickel (II) capture from complexes with NTA, EDDA, and related tetradentate chelating agents by the hexadentate chelating agents EDTA and CDTA: Evidence of a "semijunctive" ligand exchange pathway. Geochim Cosmochim Acta 2017;212:176–95.
[29] Truong KN, Müller P, Dronskowski R, Englert U. Dynamic uptake and release of water in the mixed-metal EDTA complex M_3 [$_{\gamma}$b (EDTA)(C_O3)](M = K, Rb, Cs). Cryst Growth Des 2016;17(1):80–8.
[30] Bodaghifard MA. Bis sulfamic acid functionalized magnetic nanoparticles as a retrievable nanocatalyst for the green synthesis of polyhydroquinolines and tetrahydrobenzopyrans. J Nanostruct 2019;9(1):29–40.
[31] Shi X, Yang J, Salvador JR, Chi M, Cho JY, Wang H, et al. Multiple-filled skutterudites: high thermoelectric figure of merit through separately optimizing electrical and thermal transports. J Am Chem Soc 2011;133(20):7837–46.
[32] Liu Q, Ma K, Wen D, Sun H, Wang Q, Kong J, et al. BisPNA-assisted detection of double-stranded DNA via electrochemical impedance spectroscopy. Electroanalysis 2019;31(1):160–6.

[33] Liu X, Aizen R, Freeman R, Yehezkeli O, Willner I. Multiplexed aptasensors and amplified DNA sensors using functionalized graphene oxide: application for logic gate operations. ACS Nano 2012;6(4):3553–63.
[34] Liu S, Su W, Li Z, Ding X. Electrochemical detection of lung cancer specific microRNAs using 3D DNA origami nanostructures. Biosens Bioelectron 2015;71:57–61.
[35] Yun W, Wu H, Chen L, Yang L. Dual enzyme-free amplification strategy for ultra-sensitive fluorescent detection of bisphenol A in water. Anal Chim Acta 2018;1020:104–9.
[36] Altintas Z, Tothill I. Biomarkers and biosensors for the early diagnosis of lung cancer. Sens Actuators, B 2013;188:988–98.
[37] Taghdisi SM, Danesh NM, Ramezani M, Yazdian-Robati R, Abnous K. An amplified fluorescent aptasensor based on single-stranded DNA binding protein, copper and silica nanoparticles for sensitive detection of interferon-gamma. Anal Chim Acta 2017;984:162–7.
[38] Pan L, Huang Y, Wen C, Zhao S. Label-free fluorescence probe based on structure-switching aptamer for the detection of interferon gamma. Analyst 2013;138(22):6811–6.